Using Nanotopography and Metabolomics to Identify Biochemical Effectors of Multipotency

P. Monica Tsimbouri,[†] Rebecca J. McMurray,[†] Karl V. Burgess,[‡] Enateri V. Alakpa,[†] Paul M. Reynolds,[⊥] Kate Murawski,[§] Emmajayne Kingham,[§] Richard O. C. Oreffo,[§] Nikolaj Gadegaard,[⊥,*] and Matthew J. Dalby[†,*]

[†]Centre for Cell Engineering, Institute of Molecular, Cell and Systems Biology, College of Medical, Veterinary and Life Sciences, Joseph Black Building, University of Glasgow, Glasgow, G12 8QQ, Scotland, U.K., [‡]Glasgow Polyomics Facility, Joseph Black Building, Institute of Biomedical and Life Sciences, University of Glasgow, Glasgow, G12 8QQ, Scotland, U.K., [§]Bone & Joint Research Group, Centre for Human Development, Stem Cells and Regeneration, Institute of Developmental Sciences, University of Southampton, Southampton SO16 6YD, U.K., and [⊥]Division of Biomedical Engineering, School of Engineering, University of Glasgow, Glasgow, G12 8LT, Scotland, U.K.

ABSTRACT It is emerging that mesenchymal stem cell (MSC) metabolic activity may be a key regulator of multipotency. The metabolome represents a "snapshot" of the stem cell phenotype, and therefore metabolic profiling could, through a systems biology approach, offer and highlight critical biochemical pathways for investigation. To date, however, it has remained difficult to undertake unbiased experiments to study MSC multipotency in the absence of strategies to retain multipotency without recourse to soluble factors that can add artifact to experiments. Here we apply a nanotopographical systems approach linked to metabolomics to regulate plasticity and demonstrate rapid metabolite reorganization, allowing rational selection of key biochemical targets of self-renewal (ERK1/2, LDL, and Jnk). We then show that these signaling effectors regulate functional multipotency.

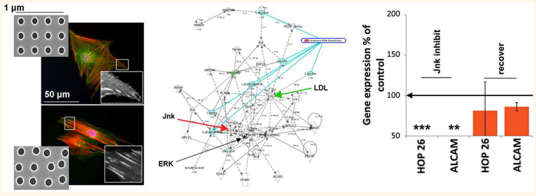

KEYWORDS: nanotopography · systems biology · mesenchymal stem cells · metabolomics

Adult stem cells in their niche remain as slow proliferating, metabolically quiescent cells in order to help maintain self-renewal. Understanding the stem cell niche is important, and exploitation of this knowledge will help develop new tissue engineering scaffolds and stem cell therapies. However, it has been problematic to produce an *in vitro* environment to compare growth, differentiation, and metabolism in differentiating and self-renewing mesenchymal stem cells (MSCs), as the appropriate experimental controls have not been available. Current strategies to manipulate stem and progenitor populations typically rely on complex and poorly understood cocktails of soluble factors that slow growth or induce cell differentiation.

Materials science presents a different approach to directing stem cell fate in the absence of chemical cues or media supplements. Researchers have presented data on the application of the cell/material interface (chemistry,[1−4] stiffness,[5] and nanotopography[6,7]) to target MSC differentiation.

More recently, MSC/materials interfacial research has shifted focus to maintenance of multipotency (as can be indicated by expression of, for example, STRO1, HOP26 (CD63), and ALCAM (CD166)).[8−10] This is important, as MSCs spontaneously differentiate *in vitro* into heterogeneous populations of differentiated cell types, mainly fibroblasts, with dwindling numbers of true stem cells during culture. Thus far, chemical patterning has been shown to allow prolonged expression of MSC marker transcripts in MSCs,[11] tuned stiffness has been demonstrated to allow increased self-renewal of muscle stem cells by mimicking elasticity of the *in vivo* niche,[12] and nanotopography has been shown to allow retained functional multipotency in MSCs.[13]

Nanotopography may be particularly useful, as the surfaces designed for targeted osteogenesis of MSCs and retention of MSC multipotency have similar chemistry, stiffness (they can be embossed into identical bulk thermoplastics), and physical properties

* Address correspondence to matthew.dalby@glasgow.ac.uk, nikolaj.gadegaard@glasgow.ac.uk.

Received for review September 2, 2012 and accepted October 16, 2012.

Published online October 16, 2012
10.1021/nn304046m

(the materials exhibit identical contact angles).[13] The retention surfaces use a square arrangement of 120 nm diameter, 100 nm deep pits with 300 nm center−center spacing (square, SQ), and the osteo-specific surfaces are similar but use a ±50 nm offset from the center position (*i.e.*, they have average 300 nm center−center spacing) (near square 50, NSQ50); otherwise they are identical. Thus, it is nanoscale cues alone that drive cell fate. Furthermore, this system allows the study of MSCs without artifact induced by changing media formulations.

It is considered that integrin regulation is important in stem cell niche function,[14] and it is accepted that osteogenesis from MSCs in response to materials is tension dependent with contraction-driving kinases such as Rho A kinase (ROCK) central to derivation of the high tensional state required for osteogenesis through activation of Rho A-initiating actin/myosin cytoskeletal contraction.[2,3]

Thus, this study starts by comparing adhesion and tension in MSC populations with retained multipotency (on SQ) and populations undergoing osteogenesis (on NSQ50). Use of the NSQ50 surface controls the experiments, as the roles of adhesion and tension in osteogenesis are well understood. This then allowed us to understand how to manipulate MSCs on the SQ surface to investigate plasticity for the first time using nanotopographies.

A few studies have shown that stem cells are metabolically inactive, in contrast to observed increased metabolic activity in stem cells undergoing active differentiation, and also that the metabolome responds to change rapidly, providing instant phenotypical information.[15,16] Thus, coupling the developed plasticity system to high-resolution mass spectrometry and pathway bioinformatics allowed use of metabolite information as a novel method to select unbiased biochemical signaling modulators of multipotency *without bias or preconception*.

RESULTS AND DISCUSSION

Osteogenesis and Multipotency Are Different Tensional States. In their niche, MSCs are considered to use many small adhesions. This is sensible considering the stiffness of the marrow is 250−750 Pa[17] and low elasticity would not support formation of large focal adhesions due to deformation of the matrix absorbing intracellular tension.[5] It could be postulated that use of smaller, more transient adhesions may permit a more dynamic interaction with basement membranes and extracellular matrix that are considered central in self-renewal and differentiation.[18,19]

However, for osteogenesis to occur, adhesions must lengthen[20] to support more contractile morphologies with higher levels of intracellular tension.[2,3] It is likely that in the niche interaction with basement membranes and extracellular matrix would regulate adhesion size and hence MSC phenotype.[18,19] In fact, the role of adhesions within the niche are considered to be quite broad, with roles in influencing stem cell homing, tethering stem cells to the niche, development of the niche architecture, regulating proliferation and self-renewal, and controlling the orientation of dividing cells.[14]

Figure 1A shows that cells on the osteogenic NSQ50 surface indeed had larger focal adhesions after 3 days of culture compared to MSCs on SQ or planar control. Figure 1B shows a phospho-myosin (p-myosin, pSer 19 chosen, as it is phosphorylated ROCK) by Western blot

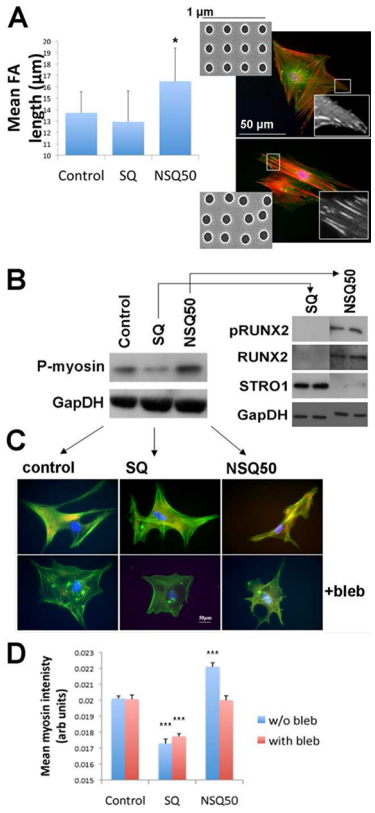

Figure 1. Adhesion, tension, and phenotype. (A) MSCs cultured on MSC-retaining SQ and osteospecific NSQ50 use different adhesion sizes. On SQ, the MSCs have small adhesions, while on NSQ50, the MSCs have significantly larger adhesions after 3 days of culture. Results are mean ± SD for at least 50 cells from 3 material replicates; * = $p < 0.05$ by ANOVA. (B) Western analysis for p-myosin shows NSQ50 to have high levels of intracellular tension, while MSCs on SQ have lower expression of p-myosin than cells on planar control. Western blot is also used to demonstrate high levels of RUNX2 and pRUNX2 expression in MSCs on NSQ50 and high levels of STRO-1 expression in MSCs on SQ, hence correlating tension and phenotype. (C) Blebbistatin treatment to inhibit myosin/actin interaction shows a reduction in p-myosin staining, with large changes in morphology particularly noted on NSQ50. Red = p-myosin, green = actin (yellow = co-localization), blue = DNA. (D) Image analysis of at least 90 cells from 3 material replicates reflects these observations with little change in intensity for MSCs on SQ and control with blebbistatin, but a large drop in p-myosin expression in MSCs on NSQ50. *** = $p < 0.001$ from control by ANOVA.

and immunofluorescence. The results clearly showed than on NSQ50 high-levels of p-myosin were expressed, whereas on SQ, low levels of p-myosin were expressed, indicating that to retain multipotency, a low level of cytoskeletal tension was required, while, as expected, to undergo osteogenesis, high levels of intracellular tension were required. Phenotypical analysis for osteogenesis (total and phosphorylated runt-related transcription factor 2, RUNX2, an osteogenic transcription factor) and MSC phenotype (STRO-1) confirmed retention of MSC phenotpye on SQ and osteogenesis on NSQ50 (Figure 1B).

Tensional state was confirmed as when blebbistatin was added to inhibit myosin function. It was seen that the MSCs on the NSQ50 collapsed to form highly stellate morphologies, demonstrating the high degree of tension they were under during osteogenesis (Figure 1C and confirmed by CellProfiler[21] analysis in Figure 1D). MSCs on SQ and control did not undergo such dramatic change, suggesting their morphology was less dependent on intracellular tension.

Creating a Plasticity "System". As described, adhesion and tension are important in MSC fate. Thus, in this report, we wish to use this knowledge to create a biological system to represent plasticity around MSCs retained in the multipotent state on the SQ topography. Blocking adhesion with integrin antibodies is a simple way of changing cell/material interaction; thus antibodies against β_1 and β_3 integrins (chosen for more broad effects than α subunits) were trialed. Using CD271 as an MSC marker[22] (Figure 2A), immunofluorescence was coupled to CellProfiler[21] to measure mean intensity (brightness, Figure 2B) and standard intensity (deviation across a cell, Figure 2C) to see which antibody reduced expression most efficiently. It was clearly seen that blockade of β_3 reduced expression significantly better than β_1. This is interesting, as β_3 has previously been implicated in nanotopographical sensing, passing topographical information into the actin cytoskeleton, while β_1 was shown not to confer nanotopographical information in the same study.[23]

To produce a biological system mimicking plasticity, we wanted a differentiation and recover scenario. Thus, a first step was to investigate the effect of β_3 blockade on tension. P-myosin Western blot and densitometry showed slight reduction in p-myosin expression in hand with a rounding of cell morphology with addition of the antibody for 3 days. Removal of the antibody appeared to return p-myosin expression to normal (Figure 2D). We acknowledge that the changes were very small, and this infers that in MSCs with a low starting intracellular tension (lower than on planar control) there is perhaps not much tension to lose, and effects could be more biochemical (we will discuss this later).

Next, MSC markers (STRO-1, ALCAM, and HOP26[22,24,25]) were investigated to see if expression could be lost and

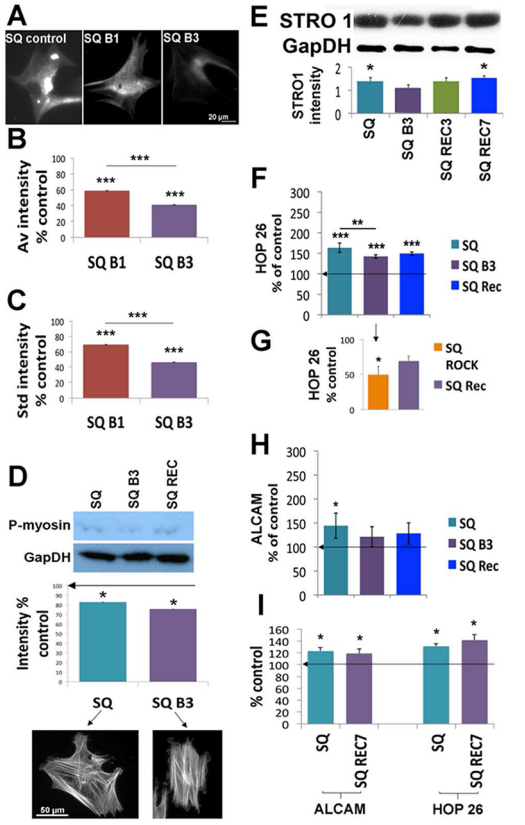

Figure 2. Creating a "plasticity system". (A–C) Influence of β_1 and β_3 integrin blocking on MSC expression of CD271. (A, B) As antibodies were added to cultures, the intensity of CD271 expression was reduced; this was most highly significant when anti-β_3 was used. (C) Similarly, expression of CD271 across the cell surface became less conformal as blocking antibodies were used, again, most notably with anti-β_3. Results are mean ± SD for at least 50 cells from 3 material replicates, *** = $p < 0.001$ by ANOVA. (D) Western blot showed addition of β_3 to MSC cultures on SQ resulted in a speculative reduction of p-myosin expression, but this was not significantly significant (densitometry from Western blots shows mean ± SD, $n = 9$ material replicates, * = $p < 0.05$ by ANOVA compared to MSCs on planar control). However, a change in morphology was noted from stellate to more rounded. (E) Western blot analysis of the MSC marker STRO-1 coupled to densitometry showed a significant reduction in expression with β_3 blocking that could be recovered if the antibody was removed and the cells allowed 7 days to recover (results are mean ± SD, $n = 9$ material replicates, * = $p < 0.05$ by ANOVA compared to MSCs on planar control). (F) Transcript analysis for HOP26 demonstrated a highly significant drop in HOP26 expression with addition of anti-β_3; the expression did not return to original levels after 3 days of recovery from blocking. (G) To help see if tension is important in this change, ROCK inhibition was used. Again, after 3 days of inhibition, a reduction in HOP26 expression was noted (100% represents MSCs on SQ with no inhibitor), and expression could be recovered 3 days after removing the inhibitor. (H) Another MSC marker, ALCAM, was also trialed. Similar to HOP26, addition of anti-β_3 reduced expression of transcript, but this did not return to normal levels after 3 days of recovery. (I) Allowing longer (7 days) time from removal of the blocking antibody for recovery provided full recovery back to original levels of HOP26 and ALCAM expression as compared to MSCs cultured on SQ with no adhesion inhibition. For qPCR graphs show mean ± SD, experimental repeats = 3 with $n = 9$ in each experiment (except for day 7-day recovery data, where $n = 9$), statistics by ANOVA * = $p < 0.05$, ** = $p < 0.01$. SQ = SQ plain culture, B3 = β_3 subunit blocked, B1 = β_1 subunit blocked, REC = recovered culture.

regained as β_3 antibody was introduced and removed. STRO-1 was investigated at the protein level by Western blot and densitometry, and it was demonstrated that after 3 days of culture on SQ high levels of STRO-1 expression were noted. Addition of β_3 antibody during this incubation significantly reduced STRO-1 expression, if the antibody was removed and replaced with normal media for 3 days, partial recovery of expression was noted, and if 7 days were allowed for recovery, similar to original levels of STRO-1 expression were noted (Figure 2E).

Quantitative real-time polymerase chain reaction (qPCR) was next used to investigate HOP26 and ALCAM expression with 3-day block and 3-day recovery. For HOP26, marker levels were significantly reduced compared to MSCs on SQ with no adhesion inhibition. With 3 days' recovery, HOP26 expression recovered slightly to having no significant difference from cells cultured on SQ (Figure 3F). Interestingly, if ROCK was inhibited (using Y27632), a similar trend was observed, suggesting a role for g-protein signaling and/or actomyosin contractility in plasticity probably linked to the change in cell morphology (rounding with addition of β_3 antibody) (Figure 2G).

qPCR for ALCAM showed a reduction in expression after 3 days of blocking, but no recovery after 3 days of antibody removal (Figure 2H). It is noteworthy that, as for the STRO-1 Western analysis, if 7 days of culture after antibody removal was allowed, complete recovery of both HOP26 and ALCAM to levels identical to those of MSCs culture on SQ in normal conditions was seen (Figure 2I).

Together, these data allow us to demonstrate use of adhesion manipulation of MSCs on a multipotency-enhancing nanotopography as a way of modeling plasticity, *i.e.*, loss and regain of MSC marker expression.

Linking Metabolism to Phenotype. In order to link metabolic activity of the MSCs to phenotype, high-resolution orbitrap mass spectrometry was performed on metabolites extracted from the cells grown on the nanotopographical surfaces with 3-day adhesion block and 3-day recovery. Total up/down-regulations were calculated and compared to respective controls as a ratio.

For MSCs cultured on SQ, a low, basal, metabolic profile was observed (Figure 3A), and this can be correlated to expression of stem cell/progenitor cell markers (STRO-1, HOP26, and ALCAM (Figure 2)). Upon integrin blocking, these markers were reduced (Figure 2) and differentiation markers (SOX9, a transcription factor indicative of chondrogenesis was used as the cells rounded with adhesion inhibition, and chondrocytes are a rounded morphology for MSCs) increased at both transcript (Figure 3B) and protein levels (Figure 3C); in line with this differentiation and loss of stem cell phenotype was a highly significant increase in metabolism (Figure 3A). As adhesion formation recovered,

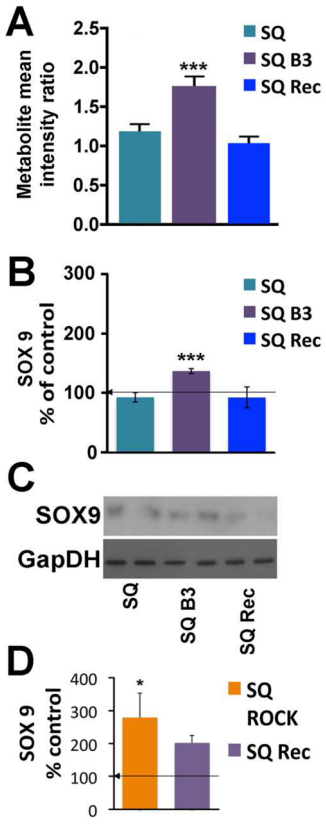

Figure 3. Linking metabolome to phenotype. (A) Total MSC metabolite values (up/down-regulations derived from mass spectrometry data for metabolites compared to appropriate control as denoted by treatment/control on the *z*-axis). For SQ, the MSC retention surface, total metabolism started low and increased with 3 days of adhesion blocking. (B for qPCR, C for Western blot) In line with this, expression of SOX9, indicative of chondrogenesis, was noted as anti-β_3 was added. Three days after adhesion inhibitors were removed from culture and as the metabolome returned to basal levels, SOX9 expression also decreased to original levels. To, again, link to tension, ROCK inhibition was used and showed an increase in SOX9 expression followed by a return to reduced expression after the inhibitor was removed. SQ = SQ plain culture, B3 = β_3 subunit blocked, REC = recovered culture. For metabolic analysis $n = 9$, results are the mean $\pm$ SD. For qPCR, graphs show mean $\pm$ SD, experimental repeats = 3 with $n = 9$ in each experiment. Statistics by ANOVA, * = $p < 0.05$, *** = $p < 0.001$.

metabolism declined to a basal state and SOX9 expression was lost (Figure 3B, C, in hand with recovering HOP26 and ALCAM expression (Figure 2)). It is important to note this is not a quiescent state, as BrdU analysis showed that after recovery from integrin blocking 12.82% of the MSCs were in S-phase. To again implicate a possible role of g-protein signaling and/or cytoskeletal contraction, ROCK inhibition was performed and SOX9 expression investigated. As with adhesion inhibition, an increase in SOX9 expression was noted as ROCK was inhibited, and this expression was lost as inhibition was ended (Figure 3D).

Dissecting the metabolomic analysis further showed metabolites involved in protein synthesis (amino acid metabolism) and energy (carbohydrate, lipid, and

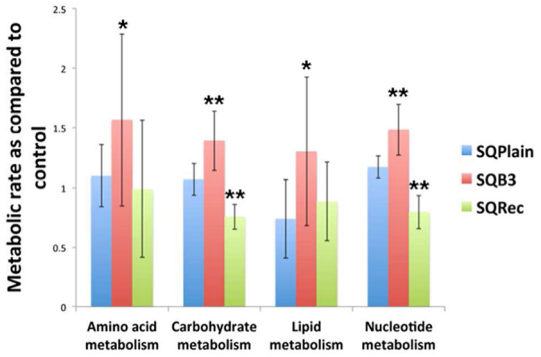

Figure 4. Analysis of metabolic pathways. Dissecting more detail from key metabolite groupings that responded strongly in our nanotopographical/adhesion system, it was seen that amino acid, carbohydrate, lipid, and nucleotide metabolism were seen to follow total metabolism closely. Each grouping started with basal expression as MSC phenotype was retained on the SQ pattern and expression was induced as adhesion was inhibited and reduced as blockade was ended (3 days inhibition, 3 days recovery). These metabolite groupings are involved in protein synthesis and energy production. Results are the mean ± SD for 9 material replicates, * = $p < 0.05$, ** = $p < 0.01$ by ANOVA.

nucleotide metabolism) closely followed the general trend with basal expression when expressing MSC markers and increased expression during differentiation (SOX9 expression) (Figure 4). More detailed metabolite information is presented in Supporting Figures S1 and S2.

Linking Metabolism to Canonical Signaling. Using Ingenuity pathway analysis (IPA) canonical and network analysis, differential regulations of key metabolic pathways could be linked to top-scoring (by numbers of up−down-regulation changes) networks. To achieve this, metabolomic data from mass spectrometry were uploaded to the Ingenuity server, and stacked metabolic pathway histograms generated along with top-ranked networks (Figure 5).

For MSCs retained as stem cells on SQ, metabolism could be seen to balance up- and down-regulations (Figure 5A) across key metabolic pathways such as amino acyl tRNA biosynthesis and the metabolism of a range of amino acids. When linked to canonical, biochemical, signaling, extracellular signal-related kinase (ERK1/2, black arrows), c-Jun N-terminal kinase (Jnk, red arrows), and low-density lipoprotein (LDL, green arrows) were highlighted as potential major signaling hubs involved in retention of multipotency (Figure 5B).

As adhesion was blocked, metabolic signaling was broadly up-regulated (Figure 5C and Figure 4B) as active differentiation (*e.g.*, to chondrocytes (Figure 3 B, C)) was initiated and, again, ERK1/2, Jnk, and LDL were indicated as signaling hubs (Figure 5D). In addition, as adhesions were allowed to re-establish, metabolic signaling was broadly down-regulated (Figure 5E) as stem cell phenotype was recovered. Once again, network analysis indicated ERK 1/2, Jnk, and LDL as key biochemical modulators (Figure 5F).

Testing of Metabolomically Selected Biochemical Targets. In order to test the validity of the data indicating ERK 1/2, Jnk, and LDL as signaling hubs for self-renewal, we used a 3-day chemical inhibition of ERK and Jnk and antibody inhibition of LDL receptor. Examination of MSC phenotype markers HOP26 and ALCAM on treated samples compared to uninhibited planar control showed expression of ALCAM and HOP26 in MSCs on SQ significantly reduced (Figure 6A−C). After 7 days of recovery from inhibition, HOP26 and ALCAM were seen to increase in expression close to original levels (Figure 6A−C).

Recognizing that use of marker expression to validate multipotency is a moot point, we selected Jnk inhibition as giving best results and then used osteogenic growth media (OGM) and adipogenic growth media (AGM) with and without Jnk inhibitor for MSCs cultured on coverslips. Results clearly demonstrated that without inhibitor the cells could be differentiated to express the adipogenic marker glucose transporter type 4 (Glut4) in AGM (Figure 6D) and the osteogenic marker osteopontin (OPN) in OGM (Figure 6E). However, with Jnk inhibited neither differentiation occurred; that is, the cells had lost their multipotential.

To help validate our approach further, gene microarrays of MSCs cultured on SQ for 3 days were used to provide an observational understanding of biochemical events. Again using Ingenuity network analysis, the top-scoring network implicated integrin signaling as a major canonical pathway, highlighted ERK1/2 as a signaling hub, and demonstrated strong up-regulation of Jnk on the multipotency-retaining surface.

It is further interesting to note that these pathways and hubs serve to down-regulate a large number of cell cycle control genes such as PRC1 (protein regulation of cytokinesis 1), Aurora A kinase (AURKA), S-phase kinase-associated protein 2 (SKP2), serine/threonine related kinase (WEE1), targeting protein for Xklp2 (TPX2), chromosome associated kinase 4A (KIF4A) and serine/threonine polo-like kinase 1 (PLK1) that are involved in cell cycle progression (*e.g.*, refs 26−31). Such targets make sense for a surface that maintains multipotency as cell cycle regulation is considered central to control of symmetrical/asymmetrical self-renewal.[14]

SUMMARY AND CONCLUSIONS

The concept of the stem cell niche was first proposed 1978 when it was reported that a stem cell may associate with other cells *in vivo* which help to regulate their behavior and maintenance.[32] However, to date, our understanding of the MSC niches remains elusive and the tools to provide a reductionist approach to dissecting the niche (*e.g.*, materials and metabolomics) are only now becoming available.

The use of nanotopography and the development of a simple system to study MSC plasticity (*i.e.*, start to differentiate and then dedifferentiate) offers an ideal

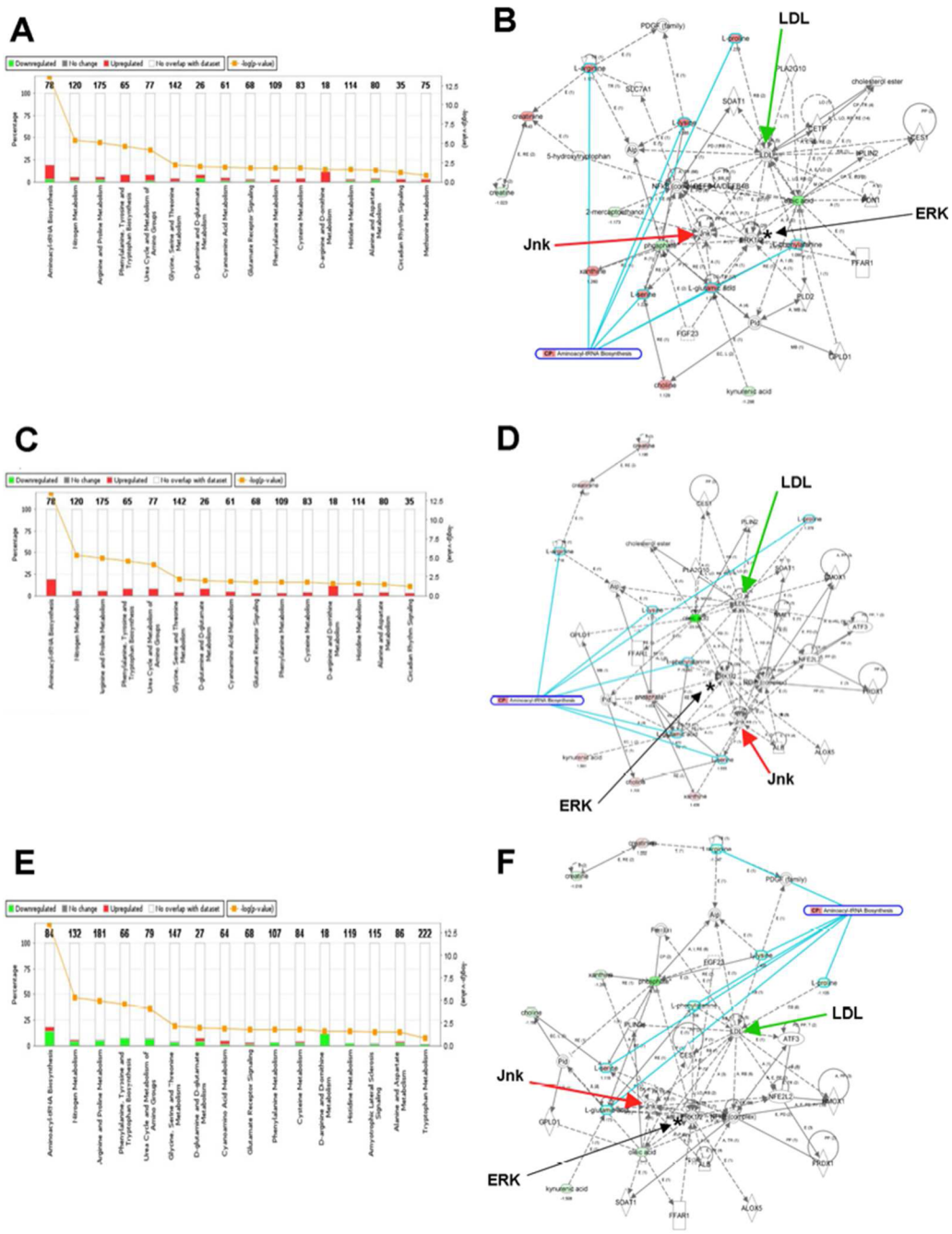

Figure 5. Metabolic pathways feed into key biochemical signaling modulators. (A) MSCs cultured on SQ retaining stem cell phenotype had a balance of up- and down-regulated metabolic signaling. (B) Many of the metabolites differentially regulated were indicated as having input into ERK1/2 (black arrow), Jnk (red arrow), and LDL (green arrow) signaling. (C) When β_3 integrin subunits were blocked, metabolic signaling was dramatically increased and, again, (D) ERK 1/2, LDL, and Jnk signaling was implicated. (E) Three days after ending integrin blocking, metabolite signaling down-regulated and, once again, (F) ERK 1/2, LDL, and Jnk signaling was implicated (n = 9).

opportunity to examine metabolomic response as a key indicator of stem cell phenotype and as a method of identifying key biochemical mediators of multipotency. Metabolite profiling will likely be of key importance in stem cell niche investigations as self-renewing stem cells are metabolically quiet[15,16] and this provides a data baseline.

Here, metabolomics based around retention of multipotency was used to indicate three unbiased (or non preselected) biochemical modulators of stem cell phenotype, ERK 1/2, Jnk, and LDL. Pharmacological inhibition of these targets in MSCs cultured on the SQ compared to planar control resulted in loss of stem cell markers that could be regained with removal of the inhibitors and furthermore, effect of functional multipotency was demonstrated. The selection was aided by `moving' the cells around the multipotent state in a "plasticity system" rather than using a static model.

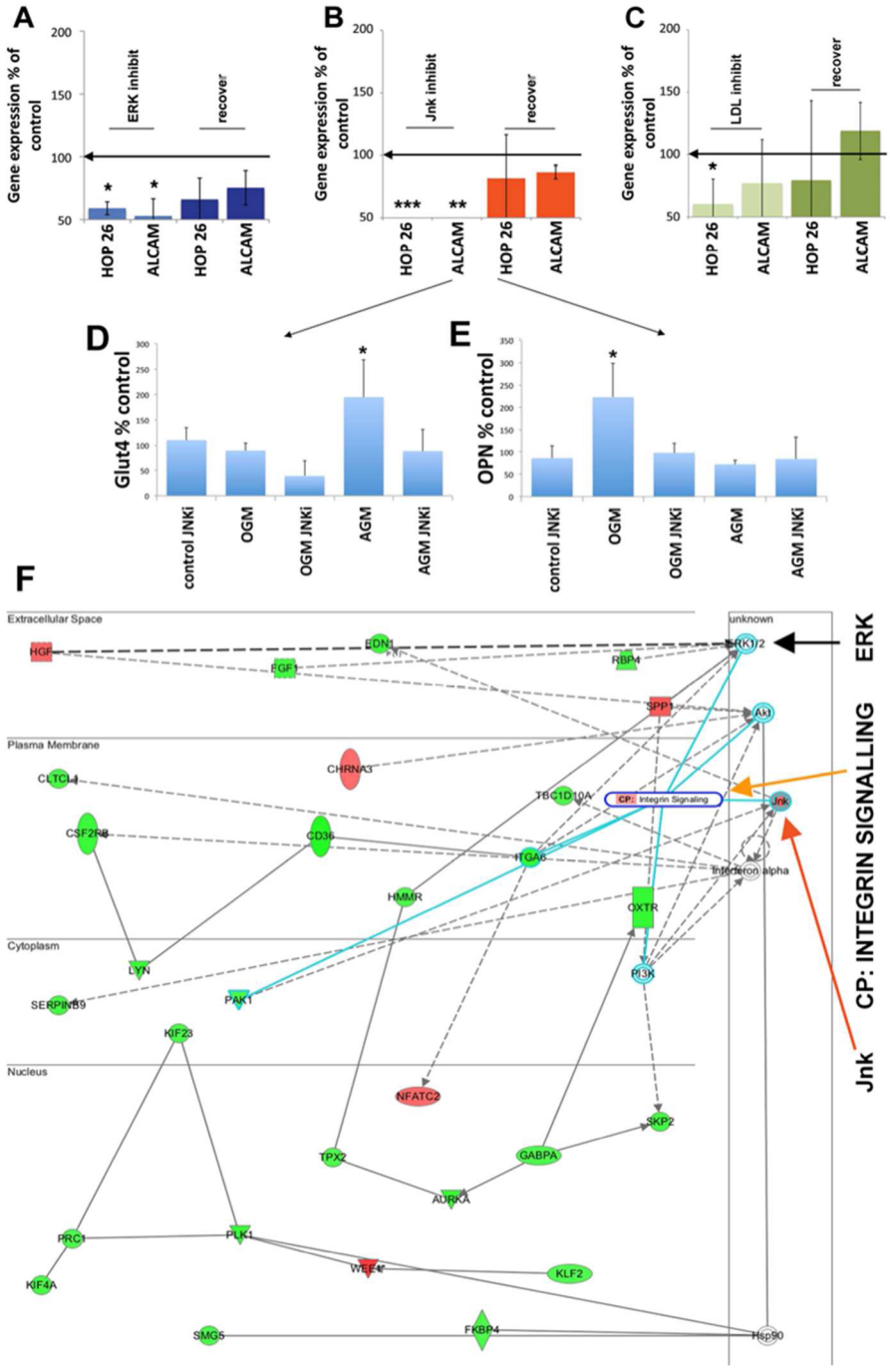

Figure 6. ERK, Jnk, and LDL inhibition effects for MSCs on SQ normalized to expression on planar control. (A) For ERK inhibition a reduction in mesenchymal stem cell markers (HOP26 and ALCAM) was seen. (B) Similarly for Jnk inhibition a reduction in mesenchymal stem cell markers (HOP26 and ALCAM) was seen. (C) For LDL receptor blocking significant down-regulation of HOP26 was noted, but while ALCAM expression was reduced, it was nonstatistically significant. As inhibition was ended for ERK, Jnk, and LDL, HOP26 and ALCAM expression was seen to increase and the difference from planar control become insignificant, demonstrating dedifferentiation. (D, E) Functional multipotency testing of MSCs on coverslips with adipogenic and osteogenic growth media (AGM and OGM, respectively) revealed that Jnk inhibition prevented differentiation to either phenotype. Results are mean ± SD for $n = 9$ material replicates, ANOVA, * = $p < 0.05$. (F) Transcript analysis by microarray implicated focal adhesion signaling as a key canonical pathway and showed ERK 1/2 and Jnk to be central signaling hubs with Jnk strongly up-regulated ($n = 3$).

Use of transcriptomics helps confirm these observations and is further interesting when correlated to p-myosin data. In the high-tension, osteo-differentiating cells, loss of tension had large effect of morphology as expected.[2,3,5] However, we showed that MSC in multipotent state on SQ[13] have intracellular tension lower than that of cells on planar control (mainly differentiating to fibroblasts). As adhesion was inhibited only small

implication for loss of intracellular tension was noted as the cells rounded and started to express SOX9. It seems more likely at this end of the tension spectrum that biochemistry has a more central role through integrin related signaling acting through ERK1/2 and Jnk. In summary, we have illustrated the usefulness of nanotopography to provide experimental controls and discovery tools in MSC studies, in this case focusing on multipotency.

We have employed the nanotopographies to take a novel approach to rational selection of biochemical targets, illustrating the potential of metabolic systems biology and added to evidence that metabolites provide a dynamic, instant indication of phenotype, much more so than transcriptomics or proteomics (note the requirement for 7 days for transcriptional and protein-level recovery of markers compared to 3 days for metabolite recovery). We thus propose this approach will provide a rapid methodology for identification of biochemical modulators removing much chance and serendipity from target selection.

Furthermore, metabolomics is attractive as sample preparation is minimal compared to, for example, RNA extraction and sensitivity is much higher than *e.g.* proteomics. These points are particularly important in materials research where novel materials tend to be of small surface area, particularly when considering the current drive toward high-throughput materials formats *e.g.* use of topoarrays,[33] arrays of stiffness[34] and spotted chemical arrays,[35,36] and so RNA/protein yield is typically very low providing requirement for time-consuming and expensive RNA amplification or saturation labeling approaches.

We finally predict that this approach will find use with other stem cell types and note that *e.g.* embryonic stem cell interactions with materials are now being highlighted and differentiation and self-renewal properties becoming understood.[37−39]

MATERIALS AND METHODS

Electron Beam Lithography. Cell culture substrates were made in a three-step process of electron beam lithography, nickel die fabrication and hot embossing.[13] Briefly, two different master substrates were fabricated to form either an array of 120 nm diameter pits of 100 nm depth and 300 nm pitch in a square (SQ) arrangement or a near-square substrate with random displacement of ±50 nm for each dot, yet maintaining an average 300 nm pitch (NSQ50). For the SQ registry, the exposure pattern was defined by a combination of the spot size, exposure dose and beam step size,[40] whereas the near square pattern was generated in custom-made code and submitted to the lithography tool. The master substrates are made on silicon substrates coated with 100 nm PMMA (Elvacite 2041, Lucite International) and then exposed using a Leica EBPG5-HR electron beam lithography tool operating at 50 kV. After exposure the substrates were developed in 1:3 MIBK:IPA for 30 s and then rinsed in copious amounts of IPA before being blown dry in a stream of nitrogen. After development, nickel dies were made directly from the patterned resist samples and a thin (50 nm) layer of Ni−V was sputter coated on the samples. This layer acted as an electrode in the subsequent electroplating process. The dies were plated to a thickness of ca. 300 μm. The process was carried out at DVDNorden in Denmark.

The nickel shims were then cleaned by stripping a protective polyurethane coating using chloroform in an ultrasound bath for 10−15 min. This was followed by a rinse in acetone and IPA before being dried with clean nitrogen gas.

Imprints of the nickel shims into polycarbonate (PC, Goodfellow UK) sheets (0.5 mm thick) were achieved on a hydraulic press (SPECAC, UK). The shim and PC were sandwiched between the plates in press and heated to 180 °C before 200 kg of force was applied. After 1 min the heating was switched off and the sandwich was allowed to cool to 70 °C before being separated. The resulting imprints, SQ and NSQ50, were trimmed for use and planar PC was used as a control substrate.

Cell Extraction and Culture. MSCs were selected from an osteoprogenitor population using a STRO1 antibody and magnetic activated cell sorting as previously described.[2] MSCs were maintained in basal media (αMEM (PAA)) supplemented with 10% FBS (PAA), 1% (v/v) 200 mM L-glutamine (Gibco), and antibiotics (6.74 U/mL penicillin-streptomycin, 0.2 μg/mL Fungizone) (PAA) at 37 °C with 5% CO_2 in a humidified incubator. Cells were seeded onto the materials at 1×10^4 cells/ml and cells cultured for 3 days. Cells were used at passages P1 − P2 throughout the study. Cells from a large number of patients were used over the course of the study to help show robustness of data.

Cell Adhesion/LDL Block and Cytoskeletal Poisoning. MSCs were counted using a hemocytometer and the required number of cells blocked with 1:1 volume of antibody to cell pellet. MSCs seeded onto the materials at 1×10^4 cells/ml and integrin β_3 (Abcam) or LDL (Epitomics) antibody was added (1:2000 dilution in the culture medium[23]) and cultured for 3 days followed by 3- or 7-day recovery period. Where cytoskeletal poisoning was required cells were cultured for 3 days in medium containing 0.5 mM acrylamide.

ERK/ROCK/Jnk Inhibition. MSCs were seeded onto the materials at 1×10^4 cells/mL. For ERK inhibition MEK inhibitor U0126 (Promega) was used at 10 μM for 3 days, for Jnk a 420119 Jnk Inhibitor II (Merck) was used at 25 μM final concentration for 3 days, and for ROCK inhibition Y27632 (Sigma) at 10 μM for 3 days; all were followed by a 7-day recovery period.

Immunofluorescence. MSCs were fixed in a 10% formaldehyde solution, permeabilized, blocked in 1% (w/v) BSA/PBS, stained with anti-STRO-1 1:50 (Sigma) or 1:200 for antivinculin (clone hVin-1, Sigma) in 1% (w/v) BSA/PBS, and incubated at 37 °C for 1 h (in conjunction with phalloidin−rhodamine, 1:200 (Molecular Probes)). Two replicas of each topography (NSQ50, SQ, FLAT) were stained in each experiment. Cells were washed 3 × 5 min in 1× PBS/0.5% Tween-20, and a biotinylated secondary anti-mouse antibody (Vector Laboratories) was added at 1:50 in 1% (w/v) BSA/PBS and incubated at 37 °C for 1 h. After washing, the samples were incubated with FITC-conjugated streptavidin (1:50, Vector Laboratories) for 30 min at 4 °C, washed, and mounted using Vectashield mountant with DAPI nuclear stain (Vector Laboratories).

Adhesion Image Analysis. For cell focal adhesion (FA) measurements the method described in ref 20 was followed. Briefly, cell images (*ca.* 50 per substrate) were exported to Adobe Photoshop, and adhesion complexes scored with a three pixel wide straight line on a layer superimposed onto the background image, creating an adhesion schematic. Analysis of individual adhesion lengths (60−400 adhesions per cell) was performed using ImageJ. We note that an alternate method for measuring cell adhesion is described in ref 41.

CellProfiler. The CellProfiler software suite (Broad Institute, USA) was used to process over 500 image sets, acquired using an inverted fluorescence microscope (Olympus). An image-processing pipeline was generated to load the DNA (DAPI), actin (phalloidin-rhodamine), and antibody stain (fluorescein),

followed by automated detection of cell nuclei, cell morphology, and marker staining intensity.

Western Blotting. MSCs were cultured on topographies for 3 days (4 biological replicas, each consisting of 4 replicas each pooled together, for each of NSQ50, SQ, and FLAT) at a density of 1×10^4 cells/mL. MSCs were lysed using protein lysis buffer (20 mM Tris-HCl, pH 7.5, 150 mM NaCl, 1 mM EDTA, 1% v/v Triton X-100) containing phosphatase and protease inhibitors (complete ULTRA Tablets, Mini, EASYpack no. 05892970001, and PhosSTOP phosphatase inhibitor cocktail tablets no. 04906845001, Roche). Protein concentration was determined using the Bradford assay (BioRad). Protein samples were run on a precast NOVEX gradient (4−12%) gel system (Invitrogen), and the samples were then transferred onto a nylon membrane (Imobilon P, Millipore) according to the manufacturer's protocol. For probing, the blots were incubated in 5% nonfat milk, PBS 0.1% (v/v), and Tween 20 with the appropriate antisera dilution. Antibodies (with dilutions) used were directed to osteogenic markers phospho-RUNX2 (Abgent no. AP3559a), 1:500 total RUNX2 (Santa Cruz Biotechnology, no. sc-10758), 1:500 stem cell marker STRO1 (Santa Cruz Biotechnology, no. sc-47733), 1:500 chondrocytic marker SOX9 (Abcam, no.ab76997), 1:1000 p-myosin (Cell Signaling, Phospho Ser 19, no. 3675), and housekeeping gene GapDH (Epitomics, no 5632-1), followed by the appropriate 1:5000 goat anti-rabbit, goat anti-mouse, or donkey anti-goat IgG HRP-conjugates (Santa Cruz). Detection was performed by enhanced chemiluminescence (Immobilon Western, Millipore).

BrdU Labeling. Following 3 days of culture on the surfaces the MSCs were washed in HEPES saline twice to remove any residual αMEM medium before adding 100 μm of BrdU/DMEM medium for 1.5 h. MSCs were washed again in HEPES saline and fixed in 4% formaldehyde/PBS. MSCs were permeabilized and blocked as described above followed by 1 h incubation with anti-BrdU/DNase (1:100) (GE Healthcare) in conjunction with actin-phalloidin. MSCs were then washed and incubated with a secondary and tertiary antibody, respectively, as above.

Quantitative Real-Time (q)PCR. MSCs were cultured on topographies for 3 days at a density of 1×10^4 cells/mL. Total RNA was extracted using a Qiagen RNeasy micro kit. Real-time qPCR was carried out and analyzed as previously described to assess the expression of RUNX2, HOP 26, ALCAM, and SOX9 (Table 1). RNA samples were reverse transcribed using the Omniscript First Strand System (Qiagen). Real-time qPCR was carried out using the 7500 real-time PCR system from Applied Biosystems. GapDH served as the housekeeping gene to normalize expression for the genes of interest. In cases where the SYBR Green method was used, primer sequences for the genes were validated by dissociation curve/melt curve analysis. Alternatively, Applied Biosystems probes were used (Table 2) using the TaqMan FAST Universal Mastermix. The GapDH housekeeping gene primer/probe set was used (ABI predesigned amplification reagent) for normalization, and primer and FAM-MGB probe sets were used for SOX9, RUNX2, and Hop 26. The $2^{-DDC}{}_T$ method[42] was used for analysis of gene expression.

Microarray. Briefly, the cells were cultured on the materials (4 material replicates) for 3 days. At these points, the cells were lysed and total RNA was extracted using a Qiagen RNeasy kit (Qiagen, UK). Gene expression changes were detected by hybridization of mRNA to Affymetrix HuGene 1.0 ST human arrays as per the manufacturer's instructions. Initial bioinformatic analysis was based on rank product,[43] and a false discovery rate of 20% was used to upload selected gene changes to the Ingenuity pathway analysis server to produce networks. IPA uses pathway libraries derived from the scientific literature.

Metabolomics. MSCs were cultured on topographies for 3 days (9 material replicates for each of NSQ50, SQ, and FLAT) at a density of 1×10^4 cells/mL. Prior to the extraction of metabolites, cells were washed in 1× PBS. Metabolites were extracted using an extraction solvent (1:3:1 chloroform/methanol/water) and placed on a rotary shaker for 1 h at 4 °C. Following this, the sample supernatant was centrifuged for 3 min at 13000*g* at 4 °C. Samples were then used (note that total protein content as measured by Nanodrop (Thermo Fisher) was identical for all samples at this time point, and thus no standardization was required) for hydrophilic interaction liquid chromatography−mass spectrometry (UltiMate 3000 RSLC (Thermo Fisher) with a 150 × 4.6 mm ZIC-HILIC column running at 300 μL/min and Orbitrap Exactive (Thermo Fisher), respectively) analysis. Raw mass spectrometry data were processed using our standard pipeline, consisting of XCMS[44] (for peak picking), MzMatch[45] (for filtering and grouping), and IDEOM[46] (for further filtering, postprocessing, and identification). Core metabolite identifications were validated against a panel of unambiguous standards by mass and retention time. Additional putative identifications were assigned by mass and predicted retention time.[47] Means and standard errors of the mean were generated for all groups of picked peaks, and the resulting data were uploaded to Ingenuity pathway analysis software for pathway analysis.

TABLE 1. qPCR Primer Details for SYBR Green

gene	forward primer	reverse primer
ALCAM	ACGATGAGGCAGACGAGATAAGT	CAGCAAGGAGGAGACCAACAAC
GapDH	GTCAGTGGTGGACCTGACCT	ACCTGGTGCTCAGTGTAGCC

TABLE 2. qPCR Details for ABI TaqMan Assays

gene	ABI TaqMan Assay ID
RUNX2	Hs00231692_m1
Sox9	Hs00165814_m1
Hop 26	Hs_00156390_m1
GapDH	4352934E

Statistics. Unless otherwise indicated, $n = 9$ material replicates and for qPCR the mean of 3 experimental sets ($n = 9$ for each) were used due to technique variability with low RNA concentrations. Statistical analysis was carried out using the Tukey−Kramer multiple-comparisons post-test analysis of variance (ANOVA) as indicated in the figure legends.

Conflict of Interest: The authors declare no competing financial interest.

Supporting Information Available: Supporting material is available free of charge *via* the Internet at http://pubs.acs.org.

Acknowledgment. This work was funded by BBSRC grant BB/G008868/1. We thank Mary Robertson for sample preparation, and we thank the orthopaedic surgeons at Southampton General Hospital for the provision of bone marrow samples.

REFERENCES AND NOTES

1. Benoit, D. S. W.; Schwartz, M. P.; Durney, A. R.; Anseth, K. S. Small Functional Groups for Controlled Differentiation of Hydrogel-Encapsulated Human Mesenchymal Stem Cells. *Nat. Mater.* **2008**, *7*, 816–823.
2. McBeath, R.; Pirone, D. M.; Nelson, C. M.; Bhadriraju, K.; Chen, C. S. Cell Shape, Cytoskeletal Tension, and Rhoa Regulate Stem Cell Lineage Commitment. *Dev. Cell* **2004**, *6*, 483–495.
3. Kilian, K. A.; Bugarija, B.; Lahn, B. T.; Mrksich, M. Geometric Cues for Directing the Differentiation of Mesenchymal Stem Cells. *Proc. Natl. Acad. Sci. U. S. A.* **2010**, *107*, 4872–4877.
4. Curran, J. M.; Chen, R.; Hunt, J. A. Controlling the Phenotype and Function of Mesenchymal Stem Cells *in Vitro* by Adhesion to Silane-Modified Clean Glass Surfaces. *Biomaterials* **2005**, *26*, 7057–7067.
5. Engler, A. J.; Sen, S.; Sweeney, H. L.; Discher, D. E. Matrix Elasticity Directs Stem Cell Lineage Specification. *Cell* **2006**, *126*, 677–689.
6. Dalby, M. J.; Gadegaard, N.; Tare, R.; Andar, A.; Riehle, M. O.; Herzyk, P.; Wilkinson, C. D.; Oreffo, R. O. The Control of

Human Mesenchymal Cell Differentiation Using Nanoscale Symmetry and Disorder. *Nat. Mater.* **2007**, *6*, 997–1003.
7. Oh, S.; Brammer, K. S.; Li, Y. S.; Teng, D.; Engler, A. J.; Chien, S.; Jin, S. Stem Cell Fate Dictated Solely by Altered Nanotube Dimension. *Proc. Natl. Acad. Sci. U. S. A.* **2009**, *106*, 2130–2135.
8. Simmons, P. J.; Torok-Storb, B. Identification of Stromal Cell Precursors in Human Bone Marrow by a Novel Monoclonal Antibody, Stro-1. *Blood* **1991**, *78*, 55–62.
9. Triffitt, J. T.; Joyner, C. J.; Oreffo, R. O.; Virdi, A. S. Osteogenesis: Bone Development from Primitive Progenitors. *Biochem. Soc. Trans.* **1998**, *26*, 21–27.
10. Stewart, K.; Monk, P.; Walsh, S.; Jefferiss, C. M.; Letchford, J.; Beresford, J. N. Stro-1, Hop-26 (Cd63), Cd49a and Sb-10 (Cd166) as Markers of Primitive Human Marrow Stromal Cells and Their More Differentiated Progeny: A Comparative Investigation *in Vitro*. *Cell Tissue Res.* **2003**, *313*, 281–290.
11. Curran, J. M.; Stokes, R.; Irvine, E.; Graham, D.; Amro, N. A.; Sanedrin, R. G.; Jamil, H.; Hunt, J. A. Introducing Dip Pen Nanolithography as a Tool for Controlling Stem Cell Behaviour: Unlocking the Potential of the Next Generation of Smart Materials in Regenerative Medicine. *Lab Chip* **2010**, *10*, 1662–1670.
12. Gilbert, P. M.; Havenstrite, K. L.; Magnusson, K. E.; Sacco, A.; Leonardi, N. A.; Kraft, P.; Nguyen, N. K.; Thrun, S.; Lutolf, M. P.; Blau, H. M. Substrate Elasticity Regulates Skeletal Muscle Stem Cell Self-Renewal in Culture. *Science* **2010**, *329*, 1078–1081.
13. McMurray, R. J.; Gadegaard, N.; Tsimbouri, P. M.; Burgess, K. V.; McNamara, L. E.; Tare, R.; Murawski, K.; Kingham, E.; Oreffo, R. O.; Dalby, M. J. Nanoscale Surfaces for the Long-Term Maintenance of Mesenchymal Stem Cell Phenotype and Multipotency. *Nat. Mater.* **2011**, *10*, 637–644.
14. Watt, F. M.; Hogan, B. L. Out of Eden: Stem Cells and Their Niches. *Science* **2000**, *287*, 1427–1430.
15. Yanes, O.; Clark, J.; Wong, D. M.; Patti, G. J.; Sanchez-Ruiz, A.; Benton, H. P.; Trauger, S. A.; Desponts, C.; Ding, S.; Siuzdak, G. Metabolic Oxidation Regulates Embryonic Stem Cell Differentiation. *Nat. Chem. Biol.* **2010**, *6*, 411–417.
16. Reyes, J. M.; Fermanian, S.; Yang, F.; Zhou, S. Y.; Herretes, S.; Murphy, D. B.; Elisseeff, J. H.; Chuck, R. S. Metabolic Changes in Mesenchymal Stem Cells in Osteogenic Medium Measured by Autofluorescence Spectroscopy. *Stem Cells* **2006**, *24*, 1213–1217.
17. Winer, J. P.; Janmey, P. A.; McCormick, M. E.; Funaki, M. Bone Marrow-Derived Human Mesenchymal Stem Cells Become Quiescent on Soft Substrates but Remain Responsive to Chemical or Mechanical Stimuli. *Tissue Eng. Part A* **2009**, *15*, 147–154.
18. Li, L.; Xie, T. Stem Cell Niche: Structure and Function. *Annu. Rev. Cell Dev. Biol.* **2005**, *21*, 605–631.
19. Scadden, D. T. The Stem-Cell Niche as an Entity of Action. *Nature* **2006**, *441*, 1075–1079.
20. Biggs, M. J.; Richards, R. G.; Gadegaard, N.; Wilkinson, C. D.; Oreffo, R. O.; Dalby, M. J. The Use of Nanoscale Topography to Modulate the Dynamics of Adhesion Formation in Primary Osteoblasts and Erk/Mapk Signalling in Stro-1+ Enriched Skeletal Stem Cells. *Biomaterials* **2009**, *30*, 5094–5103.
21. Kamentsky, L.; Jones, T. R.; Fraser, A.; Bray, M. A.; Logan, D. J.; Madden, K. L.; Ljosa, V.; Rueden, C.; Eliceiri, K. W.; Carpenter, A. E. Improved Structure, Function and Compatibility for Cellprofiler: Modular High-Throughput Image Analysis Software. *Bioinformatics* **2011**, *27*, 1179–1180.
22. Boxall, S. A.; Jones, E. Markers for Characterization of Bone Marrow Multipotential Stromal Cells. *Stem Cells Int.* **2012**, *2012*, 975871.
23. Wood, M. A.; Bagnaninchi, P.; Dalby, M. J. The Beta Integrins and Cytoskeletal Nanoimprinting. *Exp. Cell Res.* **2008**, *314*, 927–935.
24. Zannettino, A. C.; Harrison, K.; Joyner, C. J.; Triffitt, J. T.; Simmons, P. J. Molecular Cloning of the Cell Surface Antigen Identified by the Osteoprogenitor-Specific Monoclonal Antibody, Hop-26. *J. Cell Biochem.* **2003**, *89*, 56–66.
25. Mirmalek-Sani, S. H.; Tare, R. S.; Morgan, S. M.; Roach, H. I.; Wilson, D. I.; Hanley, N. A.; Oreffo, R. O. Characterization and Multipotentiality of Human Fetal Femur-Derived Cells: Implications for Skeletal Tissue Regeneration. *Stem Cells* **2006**, *24*, 1042–1053.
26. Nikonova, A. S.; Astsaturov, I.; Serebriiskii, I. G.; Dunbrack, R. L., Jr.; Golemis, E. A., Aurora a Kinase (Aurka) in Normal and Pathological Cell Division. *Cell. Mol. Life Sci.* **2012**.
27. Zhu, C.; Jiang, W. Cell Cycle-Dependent Translocation of Prc1 on the Spindle by Kif4 Is Essential for Midzone Formation and Cytokinesis. *Proc. Natl. Acad. Sci. U. S. A.* **2005**, *102*, 343–348.
28. Amati, B.; Vlach, J. Kip1Meets Skp2: New Links in Cell-Cycle Control. *Nat. Cell Biol.* **1999**, *1*, E91–93.
29. Brunet, S.; Dumont, J.; Lee, K. W.; Kinoshita, K.; Hikal, P.; Gruss, O. J.; Maro, B.; Verlhac, M. H. Meiotic Regulation of Tpx2 Protein Levels Governs Cell Cycle Progression in Mouse Oocytes. *PLoS ONE* **2008**, *3*, e3338.
30. Eisen, M. B.; Spellman, P. T.; Brown, P. O.; Botstein, D. Cluster Analysis and Display of Genome-Wide Expression Patterns. *Proc. Natl. Acad. Sci. U. S. A.* **1998**, *95*, 14863–14868.
31. Stanford, J. S.; Ruderman, J. V. Changes in Regulatory Phosphorylation of Cdc25c Ser287 and Wee1 Ser549 During Normal Cell Cycle Progression and Checkpoint Arrests. *Mol. Biol. Cell* **2005**, *16*, 5749–5760.
32. Schofield, R. The Relationship between the Spleen Colony-Forming Cell and the Haemopoietic Stem Cell. *Blood Cells* **1978**, *4*, 7–25.
33. Unadkat, H. V.; Hulsman, M.; Cornelissen, K.; Papenburg, B. J.; Truckenmuller, R. K.; Post, G. F.; Uetz, M.; Reinders, M. J.; Stamatialis, D.; van Blitterswijk, C. A.; de Boer, J. An Algorithm-Based Topographical Biomaterials Library to Instruct Cell Fate. *Proc. Natl. Acad. Sci. U. S. A.* **2011**, *108*, 16565–16570.
34. Gobaa, S.; Hoehnel, S.; Roccio, M.; Negro, A.; Kobel, S.; Lutolf, M. P. Artificial Niche Microarrays for Probing Single Stem Cell Fate in High Throughput. *Nat. Methods* **2011**, *8*, 949–955.
35. Anderson, D. G.; Levenberg, S.; Langer, R. Nanoliter-Scale Synthesis of Arrayed Biomaterials and Application to Human Embryonic Stem Cells. *Nat. Biotechnol.* **2004**, *22*, 863–866.
36. Mei, Y.; Saha, K.; Bogatyrev, S. R.; Yang, J.; Hook, A. L.; Kalcioglu, Z. I.; Cho, S. W.; Mitalipova, M.; Pyzocha, N.; Rojas, F.; Van Vliet, K. J.; Davies, M. C.; Alexander, M. R.; Langer, R.; Jaenisch, R.; Anderson, D. G. Combinatorial Development of Biomaterials for Clonal Growth of Human Pluripotent Stem Cells. *Nat. Mater.* **2010**, *9*, 768–778.
37. Irwin, E. F.; Gupta, R.; Dashti, D. C.; Healy, K. E. Engineered Polymer-Media Interfaces for the Long-Term Self-Renewal of Human Embryonic Stem Cells. *Biomaterials* **2011**, *32*, 6912–6919.
38. Chen, W.; Villa-Diaz, L. G.; Sun, Y.; Weng, S.; Kim, J. K.; Lam, R. H.; Han, L.; Fan, R.; Krebsbach, P. H.; Fu, J. Nanotopography Influences Adhesion, Spreading, and Self-Renewal of Human Embryonic Stem Cells. *ACS Nano* **2012**, *6*, 4094–4103.
39. Ji, L.; LaPointe, V. L.; Evans, N. D.; Stevens, M. M. Changes in Embryonic Stem Cell Colony Morphology and Early Differentiation Markers Driven by Colloidal Crystal Topographical Cues. *Eur. Cell Mater.* **2012**, *23*, 135–146.
40. Gadegaard, N.; Thoms, S.; MacIntyre, D. S.; McGhee, K.; Gallagher, J.; Casey, B.; Wilkinson, C. D. W. Arrays of Nano-Dots for Cellular Engineering. *Microelectron. Eng.* **2003**, *67−68*, 162–168.
41. Rivera-Gil, P.; Yang, F.; Thomas, H.; Li, L.; Terfort, A.; Parak, W. J. Development of an Assay Based on Cell Counting with Quantum Dot Labels for Comparing Cell Adhesion within Cocultures. *Nano Today* **2011**, *6*, 20–27.
42. Livak, K. J.; Schmittgen, T. D. Analysis of Relative Gene Expression Data Using Real-Time Quantitative Pcr and the 2(-Delta Delta C(T)) Method. *Methods* **2001**, *25*, 402–408.
43. Breitling, R.; Armengaud, P.; Amtmann, A.; Herzyk, P. Rank Products: A Simple, yet Powerful, New Method to Detect

Differentially Regulated Genes in Replicated Microarray Experiments. *FEBS Lett.* **2004**, *573*, 83–92.
44. Smith, C. A.; Want, E. J.; O'Maille, G.; Abagyan, R.; Siuzdak, G. Xcms: Processing Mass Spectrometry Data for Metabolite Profiling Using Nonlinear Peak Alignment, Matching, and Identification. *Anal. Chem.* **2006**, *78*, 779–787.
45. Scheltema, R. A.; Jankevics, A.; Jansen, R. C.; Swertz, M. A.; Breitling, R. Peakml/Mzmatch: A File Format, Java Library, R Library, and Tool-Chain for Mass Spectrometry Data Analysis. *Anal. Chem.* **2011**, *83*, 2786–2793.
46. Creek, D. J.; Jankevics, A.; Burgess, K. E.; Breitling, R.; Barrett, M. P. Ideom: An Excel Interface for Analysis of LC-MS-Based Metabolomics Data. *Bioinformatics* **2012**, *28*, 1048–1049.
47. Creek, D. J.; Jankevics, A.; Breitling, R.; Watson, D. G.; Barrett, M. P.; Burgess, K. E. Toward Global Metabolomics Analysis with Hydrophilic Interaction Liquid Chromatography-Mass Spectrometry: Improved Metabolite Identification by Retention Time Prediction. *Anal. Chem.* **2011**, *83*, 8703–8710.